Low dimensional solids based on Mo-6 cluster cyanides and Mn2+, Mn3+ or Cd2+ metal ions crystal chemistry, magnetic and optical properties

Gilles Daigre, Pierric Lemoine, Thi Diep Pham, Valérie Demange, Regis Gautier, Nikolay G. Naumov, Alexandra Ledneva, Maria Amela-Cortes, Noee Dumait, Nathalie Audebrand, et al.

Low Dimensional Solids based on Mo$_6$ Cluster Cyanides and Mn^{2+}, Mn^{3+} or Cd^{2+} Metal Ions: Crystal Chemistry, Magnetic and Optical Properties.

Gilles Daigre,[a] Pierric Lemoine,[a] Thi Diep Pham,[a] Valérie Demange,[a] Régis Gautier,[a] Nikolay G. Naumov,[b,c] Alexandra Ledneva,[b] Maria Amela-Cortes,[a] Noée Dumait,[a] Nathalie Audebrand,*[a] Stéphane Cordier*[a]

Five new cluster compounds based on [Mo$_6$Br$^i_8$(CN)$^a_6$]$^{2-}$ and [Mo$_6$Br$^i_6$Q$^i_2$(CN)$^a_6$]$^{n-}$ (Q = S, Se, n = 3, 4) cluster units have been synthetized and characterized. Structures were determined by X-ray single crystal diffraction techniques and relevant magnetic susceptibility and optical properties measurements were carried out. [*trans*-Mn(H$_2$O)$_2$][Mo$_6$Br$_8$(CN)$_6$] (**1**) crystallize in the orthorhombic system (*Imma* space group) and contain 2D square-net-layers built-up from [Mo$_6$Br$^i_8$(CN)$^a_6$]$^{2-}$ and [*trans*-M(H$_2$O)$_2$]$^{2+}$ moieties. Cs$_x$[*trans*-(Mn$^{II}_x$Mn$^{III}_{1-x}$)(H$_2$O)$_2$][Mo$_6$Br$_6$Q$_2$(CN)$_6$] (Q = S (**2**) and Se (**3**)) crystallize in the *Imma* space group as well; their structures are strongly related to that of (**1**) with a 2D square net of cluster units and transition metals. They are based on [Mo$_6$Br$^i_6$Q$^i_2$(CN)$^a_6$]$^{3-}$ (Q = S, Se) cluster units whose charge is counter balanced by Cs$^+$ as well as Mn^{2+} and Mn^{3+} in high spin states. It is evidenced that the *x* content of Cs$^+$ counter-cation is equal to that of Mn^{2+} in order to maintain - along with (1-*x*) Mn^{3+} - 23 valence electrons per cluster and a 3- charge for the cluster unit. The two oxidation states Mn^{2+} and Mn^{3+} were confirmed by electron energy loss spectroscopy (EELS) measurements. (H$_3$O)H[*cis*-Cd(H$_2$O)$_2$][Mo$_6$Br$_6$Q$_2$(CN)$_6$]·H$_2$O (Q = S (**4**) and Se (**5**)) crystallize in the trigonal system (*P*3$_1$21 space group) and are based on [Mo$_6$Br$^i_6$Q$^i_2$(CN)$^a_6$]$^{4-}$ (Q = S, Se) cluster units. In contrast to compounds **1-3**, owing to the *cis*-position of the two water molecules around the transition metal, **4** and **5** exhibit a close-packed 3D structure based on an interpenetrated framework of cluster-based chains. In particular, it contains infinite chains alternating [Mo$_6$Br$^i_6$Q$^i_2$(CN)$^a_6$]$^{4-}$ and H$^+$ protons as linkers. Magnetic and optical properties are also reported as well as theoretical calculations to support the structural analysis and physical properties. Structural analogies with [Re$_6$Q$^i_8$(CN)$^a_6$]$^{4-}$ based compounds are discussed.

1. Introduction

The chemistry of Mo$_6$ and Re$_6$ metal atom clusters is widely developed and very rich since it ranges from the solid state chemistry for the synthesis of pure inorganic compounds[1-5] to the solution and coordination chemistry for the elaboration of hybrid molecular assemblies and nanomaterials.[4, 6-8] These clusters are associated with eight face-capping ligands (L^i; i for inner) and six terminal ligands (L^a; a for apical) to form [M$_6$L$^i_8$L$^a_6$]$^{n-}$ units.[9] They exhibit unique physico-structural properties: deep red luminescence with a large Stockes shift[10-12 13 14], catalysis and photocatalysis[15-18], singlet oxygen generation[19-23], luminescence sensitizing.[24] Functionalizing M$_6$ clusters by a judicious choice of apical ligands enables to form tailored building blocks with enhanced luminescence properties[20, 25] or provides improved integration properties in matrices that can be organic (e.g. polymers[7, 24, 26, 27], liquid crystals[27-33]) or inorganic (e.g. SiO$_2$ nanoparticles[34]). Hexacyano building blocks with orthogonal position of CN groups are easily obtained with Re$_6$ clusters[9] and even with edged-bridged Nb$_6$ clusters.[35] Indeed, the chemistry of rhenium cyanides has been much studied giving rise to a wide library of extended polymeric solids by crystallization with *d* or *f* transition elements.[36-50] Crystal structure analysis of these cyanides enabled to establish some guidelines. First, an interesting feature is that cluster analogues of many metal cyanide structure types have been obtained by replacing a [M(CN)$_6$] complex by a [Re$_6$S$^i_8$(CN)$^a_6$]$^{3-/4-}$ cluster unit. Second, the choice of counter cations and their solvated species along with the charge of Re$_6$ cluster unit (3- or

4-) is the driving force for the formation of structures with defined dimensionalities. Bennett *et al*. discussed analogies between 1D framework (NPr$_4$)$_2$[Mn(H$_2$O)$_4$][Re$_6$S$_8$(CN)$_6$]·4H$_2$O and (NMe$_4$)$_2$[Mn(H$_2$O)$_4$][Fe(CN)$_6$]·4H$_2$O, 2D Cs$_2$[Mn(H$_2$O)$_2$][Re$_6$S$_8$(CN)$_6$] layered framework and Na$_2$Cu[Fe(CN)$_6$]·10H$_2$O as well as 3D Ga[Re$_6$S$_8$(CN)$_6$]·6H$_2$O, Fe$_4$[Re$_6$S$_8$(CN)$_6$]$_3$·36H$_2$O and Ni$_3$[Re$_6$S$_8$(CN)$_6$]$_2$·34H$_2$O extended frameworks with expanded Prussian Blue Ga[Fe(CN)$_6$]·xH$_2$O, Fe$_4$[Fe(CN)$_6$]$_3$·14H$_2$O and Ni$_3$[Fe(CN)$_6$]$_2$·14H$_2$O, respectively.[39] In the latter case, porosity is enhanced by the replacement of [Fe(CN)$_6$]$^{n-}$ complex with the larger [Re$_6$S$^i_8$(CN)$^a_6$]$^{n-}$ cluster unit. Although based on the isostructural [M$_6$L$^i_8$L$^a_6$]$^{n-}$ units, the chemistry of Mo$_6$ hexacyano cluster has been much less developed than the Re$_6$ one and hitherto only one layered compound has been obtained.[51] Luminescent and magnetic properties of cluster-based compounds originate from the number of metallic electrons available for metal-metal bonding (VEC = Valence Electron Count) considering in a first approximation an electronic transfer from cations to the cluster and from the cluster to the ligands. Indeed, [Mo$_6$X$^i_8$X$^a_6$]$^{2-}$ (X = halogen) is isoelectronic with [Re$_6$Q$^i_8$X$^a_6$]$^{4-}$ (Q = chalcogen), both exhibiting 24 electrons per M$_6$ cluster. To maintain the VEC equal to 24, replacing inner halogen by chalcogen around the Mo$_6$ cluster induces an increase of the charge of the cluster. Consequently, [Mo$_6$X$^i_8$X$^a_6$]$^{2-}$ is isoelectronic with [Mo$_6$X$^i_7$Q^{i}X$^a_6$]$^{3-}$ and [Mo$_6$X$^i_6$Q$^i_2$X$^a_6$]$^{4-}$ (Q = S, Se). At first glance, numerous compounds based on [Mo$_6$X$^i_6$Q$^i_2$X$^a_6$]$^{4-}$ should be isostructural with those containing the [Re$_6$Q$^i_8$X$^a_6$]$^{4-}$ cluster unit. However, other considerations must also be taken into account as for

instance the size of the units and their reactivity in aqueous solution. For instance, contrary to Re_6 clusters units, Mo_6 species easily precipitate in water to form aqua or aqua-hydroxo complexes.[52-54] Recently the photocatalytic and photovoltaic activities of Mo_6 clusters have been demonstrated[15, 17,55] offering new perspectives in the possible applications of face-capped Re_6 and Mo_6 clusters. However, Mo_6 clusters appear more competitive than Re_6 for their integration in functional materials owing to the abundance and lower price of molybdenum metal. The possibility to associate structural characteristics of layered compounds or 3D frameworks with controlled porosity and photocatalytic activities of Mo_6 clusters is particularly relevant for the development of new photocatalysts. Moreover, the association of magnetic clusters with $3d$ metal ions may lead to magnetic interactions. This work deals with the investigations on the engineering of hexacyano Mo_6 cluster based 2D and 3D extended solids using two different building blocks, namely $[Mo_6Br^i_8(CN)^a_6]^{2-}$ and $[Mo_6Br^i_6Q^i_2(CN)^a_6]^{3-, 4-}$ (Q = S, Se). Recently, we reported the structures of $[trans-Cd(H_2O)_2][Mo_6Br^i_8(CN)^a_6]$,[51] $[\{Zn(H_2O)(en)_2\}\{Zn(en)_2\}-Mo_6Br^i_6Se^i_2(CN)^a_6].2H_2O$ and of $[\{Cu(H_2O)(en)_2\}_2-Mo_6Br^i_6Se^i_2(CN)^a_6].2H_2O^{56}$ (en = ethylenediamine) that are strongly structurally related to those of $Cs_2[trans-Cd(H_2O)_2][Re_6Q^i_8(CN)^a_6]$,[37] $[\{Zn(H_2O)(en)_2\}\{Zn(en)_2\}-Re_6Te^i_8(CN)^a_6].3H_2O^{46}$ and $[Ni(NH_3)_4(en)]_2[[Ni(NH_3)_4Re_6Te^i_8(CN)^a_6].2H_2O$,[57] respectively. We also showed the stabilization of Ni^{2+} dimers in Prussian blue derivatives built up from $[Mo_6Br^i_6Q^i_2(CN)^a_6]^{4-}$ (Q = S and Se).[58] At low temperature, magnetic coupling between Ni^{2+} within the dimer occurs. Here, we report on the synthesis and the crystal structures of five new compounds based on $[Mo_6Br^i_8(CN)^a_6]^{2-}$ (1), $[Mo_6Br^i_6Q^i_2(CN)^a_6]^{3-}$ (2, 3) and $[Mo_6Br^i_6Q^i_2(CN)^a_6]^{4-}$ (4, 5) (Q = S, Se) cluster units and different transition metals. Structural features that drive the dimensionality and porosity of final compounds are discussed. Magnetic and optical properties are also reported as well as theoretical calculations to support the structural analysis and physical properties.

2. Experimental

Materials, synthesis and crystal growth.

All the compounds have been obtained following a multi-step synthesis. First the $MoBr_2$ cluster compound is synthesized by placing Mo powder (Plansee) under Br_2 gas flow according to a described procedure.[4] Then, $MoBr_2$ and KCN (Alfae Aesar, 97 %) are introduced in stoichiometric proportions in a Schlenk tube and solubilized in methanol to form $K_2[Mo_6Br^i_8(CN)^a_6]$ following a previous described procedure.[51] $K_2[Mo_6Br^i_8(CN)^a_6]$ is then used as precursor to synthesize 1. For the preparation of the chalcogen-containing precursor (Q = S or Se), $MoBr_2$, CsBr (Alfa Aesar, 99.9%), Mo (Plansee) and S or Se (Alfa Aesar, 99.999%) are introduced in stoichiometric proportions in a vacuum sealed tube and heated at 1100°C and 900°C for two days to form $Cs_4[Mo_6Br^i_6S^i_2Br^a_6]$ and $Cs_4[Mo_6Br^i_6Se^i_2Br^a_6]$, respectively, as reported elsewhere.[75] $Cs_2K_2[Mo_6Br^i_6Q^i_2(CN)^a_6]$ (Q = S, Se)

compounds are obtained from the latter $Cs_4[Mo_6Br^i_6Q^i_2Br^a_6]$ using a method previously described[56] and were used as precursors for the synthesis of 2, 3, 4 and 5. As already evidenced,[75] only the composition $[Mo_6Br^i_6Q^i_2(CN)^a_6]$ is obtained after ligands exchange reaction from the $Cs_4Mo_6Br^i_6Q^i_2Br^a_6$ solid state compounds. These results were based in particular on Se NMR and electrochemistry investigations. All other reagents are used as purchased. Elementary analyses for the heavy atoms were carried out by Electron Dispersion Spectroscopy (EDS) with a scanning electron microscope JSM 7100F. No trace of K was detected in all final compounds. Infrared spectra were recorded on a Bruker Equinox 55 FTIR spectrometer on transmittance with KBr as reference.

$[trans-Mn(H_2O)_2][Mo_6Br^i_8(CN)^a_6]$ (1). The reaction was carried out in a narrow-diameter tube by layering a solution of $K_2[Mo_6Br^i_8(CN)^a_6]$ (2.0 mg, 1.38 µmol) in water (2mL) on the top of a solution of $MnCl_2$ (STREM CHEMICALS 97%) (6mg, 48 µmol) in water (2mL). After three days at room temperature, orange crystals were obtained. Yield: 0.8 mg (0.55 µmol) (40 %). EDS analysis (at.%): Mn, 7; Mo, 40; Br, 53; K, 0. Calculated for $[trans-Mn(H_2O)_2][Mo_6Br_8(CN)_6]$: Mn, 6.7; Mo, 40; Br, 53.3. 1 is characterized by a vCN band at 2123 cm^{-1}, δHOH at 1620 cm^{-1} and vOH at 3421 cm^{-1}.

$Cs_{0.680(4)}[trans-(Mn^{II}_{0.680(4)}Mn^{III}_{0.320(4)})(H_2O)_2][Mo_6Br^i_6S^i_2(CN)^a_6]$ (2). A solution of $Mn(CH_3COO)_2.4H_2O$ (Aldrich 99%) (70 mg, 0.29 mmol, 5 ml) was slowly added to a solution of $Cs_2K_2[Mo_6Br_6S_2(CN)_6]$ (20 mg, 12 µmol, 5 ml) in a beaker and heated until 75°C. After 10 minutes under stirring at 75°C, the solution was let under gentle evaporation. Red crystals were formed within two hours along with an amorphous precipitate. Single crystals were manually extracted from the solution and washed with aliquots of water. Yield: 12 mg (8.4 µmol) (62 %). EDS analysis (at.%): Cs, 4.5; Mn, 7; Mo, 36.5; Br, 40; S, 12; K, 0. Calculated for $Cs_{0.68}[trans-(Mn^{II}_{0.68}Mn^{III}_{0.32})(H_2O)_2][Mo_6Br_6S_2(CN)_6]$: Cs, 4.3; Mn, 6.4; Mo, 38.2; Br, 38.2; S, 12.9. 2 is characterized by two vCN bands at 2107 and 2142 cm^{-1}, δHOH at 1616 and 1589 cm^{-1} and vOH at 3421 cm^{-1}.

$Cs_{0.820(4)}[trans(Mn^{II}_{0.820(4)}Mn^{III}_{0.180(4)})(H_2O)_2][Mo_6Br^i_6Se^i_2(CN)^a_6]$ (3) was synthesized as for 2 by using $Cs_2K_2[Mo_6Br^i_6Se^i_2(CN)^a_6]$ (20 mg, 11.6 µmol, 5 ml) as cluster precursor. After heating for two hours red crystals were mixed with an amorphous precipitate. Crystals were manually extracted from the solution and washed with aliquots of water. Yield: 13 mg (8.5 µmol) (73 %). EDS analysis (at.%): Cs, 4.5 ; Mn, 5.5 Mo, 36.5 ; Br, 40 ; Se, 13.5; K, 0. Calculated for $Cs_{0.82}[trans-(Mn^{II}_{0.82}Mn^{III}_{0.18})(H_2O)_2][Mo_6Br_6Se_2(CN)_6]$: Cs, 5.2; Mn, 6.3; Mo, 37.9; Br,37.9; Se, 12.7. 3 exhibits the vCN bands at the same position as 2 (2107 and 2142 cm^{-1}), δHOH at 1605 and 1561 cm^{-1} and vOH at 3416 cm^{-1}.

$(H_3O)H[cis-Cd(H_2O)_2[Mo_6Br^i_6S^i_2(CN)^a_6]-H_2O$ (4). The reaction was carried out in a narrow-diameter tube by layering a solution of $Cs_2K_2[Mo_6Br^i_6S^i_2(CN)_6]$ (2.0 mg, 1.23 µmol) in water (2 mL) on top of a solution of $CdCl_2.2H_2O$ (Merck 98%) (8 mg, 24 µmol) in

water (2 mL). After two days at room temperature, orange crystals were obtained. Yield: 1 mg (0.68 μmol) (56 %) EDS analysis (at.%): Cd, 7; Mo, 39.5; Br, 40; S, 13.5; K, 0. Calculated for $\{(H_3O)H[cis\text{-}Cd(H_2O)_2[Mo_6Br_6S_2(CN)_6]\}$: Cd, 6.7; Mo, 40; Br, 40; S, 13.3. **4** and **5** are characterized by two νCN bands at 2105 and 2141 cm^{-1}, δHOH at 1620 and 1594 cm^{-1} and νOH at 3429 cm^{-1}.

$(H_3O)H[cis\text{-}Cd(H_2O)_2[Mo_6Br^i_6Se^i_2(CN)^a_6]\text{-}H_2O$ (5) was synthesized using the same procedure as for **4**, but $Cs_2K_2[Mo_6Br^i_6Se^i_2(CN)^a_6]$ (2.0 mg, 1.2 μmol) was used as cluster precursor. After two days at room temperature, orange crystals were obtained. Yield: 1.1 mg (0.71 μmol) (53 %)

EDS analysis (at.%): Cd, 7.5; Mo, 38.5;Br, 42; Se, 12; K, 0. Calculated for $\{(H_3O)H[cis\text{-}Cd(H_2O)_2[Mo_6Br_6Se_2(CN)_6]\}$: Cd, 6.7; Mo, 40; Br, 40; Se, 13.3. IR : 2105 and 2141 cm^{-1} (νCN), 1620 and 1594 cm^{-1} (δHOH) and 3429 cm^{-1} (νOH).

Crystal structure determinations.

Crystallographic data, details on data collections and refinement parameters of the crystal structures are summarized in Table 1 and atomic coordinates, relevant selected bond lengths and angles in Tables S1(A,B)-S3(A,B). Single-crystal X-ray diffraction data were collected at 150 K on a D8 VENTURE Bruker AXS diffractometer and processed with the APEX 3 program suite[59] for compounds **1**, **2**, **4** and **5**. For compound **3**, data were collected at room temperature on an APEX-II Bruker AXS diffractometer and processed with the APEX 2 program suite.[60] For all compounds the X-ray wavelength used was the Mo-Kα (λ = 0.71073 Å). Frames integration and data reduction were carried out with the program SAINT.[61] The program SADABS [62] was employed for multiscan-type absorption corrections. Structures were determined by direct method using the SHELXT program,[63] and refined with full-matrix least-square methods based on F^2 (SHELXL-2014)[64] through the aid of the WinGX platform.[65] The quality of the data for **4** and **5** did not allow localizing the hydrogen atoms of water molecules and H_3O^+ counter-cations and the hydrogen atoms located between CN groups. The final refinements included anisotropic displacement parameters for the non-hydrogen atoms, except for some C and N atoms in **4** and **5**. Representation of asymetric units and atomic displacement ellipsoids in the structures of **1**-**5** are given in ESI (Fig. S1-S5).

Magnetic measurements.

Magnetic measurements were carried out on a SQUID magnetometer (MPMS XL5, Quantum Design) for **2** and **3**. 37.7 mg of **2** and 29 mg of **3** were wrapped in Teflon tape. The magnetic susceptibility measurements on these compounds were carried out with an applied magnetic field of 1000 Oe over the temperature range 2-300 K with a zero-field cooling procedure. Data were corrected from the diamagnetic contributions of the atomic cores.

Emission properties.

Emission spectra were recorded on solid state samples with a Nikon 80i polarized microscope equipped with a Linkam LTS420 hot stage, a Nikon Intensilight irradiation source, a Nikon DS-FI2 digital camera and an ocean optics QE6500 photodetector connected by optical fiber. An optical filter was used to select the excitation wavelengths to a bandwidth of 330-380 nm.

Reflectance spectra. Diffuse reflectance spectra were collected using a Varian Cary 100 Scan spectrometer equipped with the Varian WinUV software and a Labsphere integrating sphere (DRC-CA-30I). Experimental data were collected within the 250–800 nm range with 1 nm step and 0.5 s integration time.

Electron energy loss spectroscopy measurements.

Electron energy loss spectroscopy (EELS) was performed on compounds **2** and **3**, and for comparison, on commercial manganese oxides powders with different Mn oxidation states: MnO (Mn^{2+}, Aldrich, 99 %) Mn$_2O_3$ (Mn^{3+}, Aldrich, 99 %) and Mn$_3O_4$ (Mn^{2+}Mn$^{3+}_2$, Aldrich, 97 %). The EELS spectra were acquired on a Jeol transmission electron microscope (LaB$_6$ filament), operating at 120 eV, and equipped with a GIF (Gatan Imaging Filter) Quantum SE spectrometer. The spectral resolution, determined by measuring the half-maximum full width of the zero-loss peak was 0.65 eV, with an entrance aperture of 2.5 mm, a camera length of 8 cm and a dispersion value of 0.05 eV/ch.

Theoretical calculations.

Spin-polarized density functional theory were carried out with the CASTEP 16.1 code[66] by using the PBE functional.[67] Dispersion corrections were added in the calculations following the procedure proposed by Tkatchenko and Scheffler.[68] The convergence was reached with a minimum cut-off energy of 500 eV. A 2 × 2 × 2 *k* point grid was used to sample the Brillouin zone. All ultra-soft pseudopotentials were generated by using the OTF ultrasoft pseudo-potential generator included in the code. Relativistic effects were included for all elements during the US-PP generation by solving the radial scalar relativistic equation of Koelling and Harmon.[69, 70] During the geometry optimization, both cell parameters and atomic positions were free to relax.

3. Results and Discussion

Crystal structure of 1.

1 crystallizes in the orthorhombic system, *Imma* space group (n°74) with refined unit cell parameters *a* = 19.5758(7) Å, *b* = 10.4102(4) Å, *c* = 13.7808(5) Å, *V* = 2808.4(2) Å^3. Mo2, Br2, C2 and N2 fully occupy general 16*j* Wyckoff positions. Mo1, Br1, Br3, C1 and N1 fully occupy 8*i* (x, ¼, z) Wyckoff positions with *C$_s$* symmetry and Mn, O1 and O2 fully occupy 4*e* (0, ¼, z) Wyckoff positions with *C$_{2v}$* symmetry (Table S1A). **1** is built up from $[Mo_6Br^i_8(CN)^a_6]^{2-}$ cluster units where the face-capping positions of the octahedral cluster are fully occupied by eight bromine while the six apical positions are by cyanide ligands as depicted in Fig. 1. **1** is isostructural with [*trans*-Cd(H$_2$O)$_2$][Mo$_6$Br$_8$(CN)$_6$][51]

(a = 19.7050(7) Å, b = 10.6047(3) Å, c = 13.7982(5)Å and V = 2883.3(2) Å^3). Relevant selected bond lengths and angles are listed in Table S1B. The average Mo-Mo distances are 2.6346(1). The Mo-Br distances range from 2.586(1) to 2.596(2) Å. These distances are within the range observed in [*trans*-Cd(H$_2$O)$_2$][Mo$_6$Br$_8$(CN)$_6$][51] which is built up from the same [Mo$_6$Br$^i_8$(CN)$^a_6$]$^{2-}$ cluster unit. Note that during this work, we obtained [*trans*-Fe(H$_2$O)$_2$][Mo$_6$Br$_8$(CN)$_6$] isostructural with **1** and [*trans*-Cd(H$_2$O)$_2$][Mo$_6$Br$_8$(CN)$_6$]. It crystallizes in *Imma* space group with the following unit cell parameters: a = 19.473(4) Å, b = 10.317(2) Å, c = 13.749(3) Å, V = 2762(1) Å^3. Despite interatomic distances in agreement with those found in **1** and [*trans*-Cd(H$_2$O)$_2$][Mo$_6$Br$_8$(CN)$_6$] taking into account evolution of ionic radii of cations, owing to the poor quality of single crystals, high electronic negative and positive density peaks remained and refinements did not allow to reach satisfactory structural reliable factors for publication. Structural informations about [*trans*-Fe(H$_2$O)$_2$][Mo$_6$Br$_8$(CN)$_6$] are available on quoting CCDC 1578316.

Table 1 Crystal data and structure refinement parameters for **1–5**.

|	1	2	3	4	5
Empirical Formula	$C_6H_4MnN_6O_2Mo_6Br_8$	$C_6N_6H_4O_2Cs_{0.68}Mn^{II}_{0.68}$ $Mn^{III}_{0.32}Mo_6Br_6S_2$	$C_6N_6H_4O_2Cs_{0.82}Mn^{II}_{0.82}$ $Mn^{III}_{0.18}Mo_6Br_6Se_2$	$C_6H_{10}CdN_6O_4Mo_6Br_6S_2$	$C_6H_{10}CdN_6O_4\,Mo_6Br_6Se_2$
Formula weight (g.mol^{-1})	1461.94	1456.65	1569.05	1461.79	1555.57
Crystal size (mm^3)	0.094×0.089×0.042	0.20×0.14×0.08	0.20×0.15×0.05	0.05×0.04×0.02	0.12×0.11×0.08
Crystal color	Orange	Red	Red	Orange	Orange
Crystal system	Orthorhombic	Orthorhombic	Orthorhombic	Trigonal	Trigonal
Space group	*Imma*	*Imma*	*Imma*	*P3$_1$21*	*P3$_1$21*
a (Å)	19.5758(7)	19.5490(8)	19.616(1)	13.2013(6)	13.2807(5)
b (Å)	10.4102(4)	10.3084(4)	10.2909(7)		
c (Å)	13.7808(5)	13.7398(5)	13.8615(8)	14.1296(6)	14.1753(6)
V (Å^3)	2808.4(2)	2768.8(2)	2798.2(3)	2132.5(2)	2165.2(2)
Z	4	4	4	3	3
ρ(calcd.) (g.cm^{-3})	3.448	3.483	3.714	3.391	3.556
μ (mm^{-1})	14.42	12.770	15.272	11.896	14.093
F(000)	2604.0	2600	2776	1956	2064
λ (Å)	0.71073	0.71073	0.71073	0.71073	0.71073
T (K)	150	150	296	150	150
2Θ range (°)	2.96 to 27.49	3.46 to 40.35	2.46 to 27.51	2.29 to 27.47	2.28 to 27.52
Collected reflections	13490	15682	4299	8908	8186
Independent reflections	1749	4642	1742	3250	3283
Observed refl. [I > 2σ(I)]	1709	3353	1274	2238	2963
No. restrains / Refined parameters	0 / 80	0 / 88	0 / 85	1 / 131	2 / 130
Refined Flack parameter	-	-	-	0.38(4)	0.27(3)
Goodness-of-fit (F^2)	1.367	1.052	1.015	1.072	1.062
R_{int}, R_σ	0.024, 0.016	0.035, 0.041	0.032, 0.044	0.087, 0.123	0.056, 0.060
$R1$, $wR2$	0.055, 0.127	0.038, 0.104	0.030, 0.065	0.058, 0.127	0.051, 0.117
$R1$, $wR2$ (all data)	0.056, 0.128	0.064, 0.112	0.050, 0.070	0.088, 0.135	0.057, 0.121
(ρ_{max}, ρ_{min} / e-·Å^{-3})	2.309, -2.091	3.638, -2.197	1.697, -1.386	1.560, -1.676	1.773, -1.236
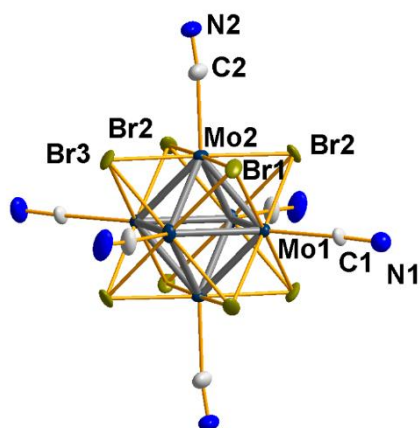
Fig 1 Representation of the [Mo$_6$Br$^i_8$(CN)$^a_6$]$^{2-}$ cluster unit in **1**. Displacement ellipsoids are shown at the 50 % probability level.

The main characteristic of these compounds is that the transition metal (M = Mn, Cd and Fe) is coordinated by four [Mo$_6$Br$_8$(CN)$^a_6$]$^{2-}$ cluster units and two water molecules localized in *trans* position (Fig. 2) leading to a 2D extended polymeric square-net-layer (Fig. 3a).
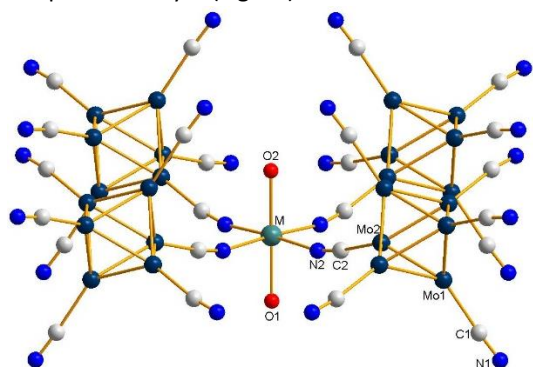
Fig. 2 Representation of the transition metal environment in **1**. Bromine ligands have been omitted for clarity.

These square-net-layers are stacked along the *c* direction, following a AA'AA' stacking type (Fig. 3b). Square-net-layers are shifted one from each other by *a*/2 translation. The structure of **1** and [*trans*-Cd(H$_2$O)$_2$][Mo$_6$Br$_8$(CN)$_6$] are strongly related to that of Cs$_2$[*trans*-M(H$_2$O)$_2$][Re$_6$S$_8$(CN)$_6$] (M = Mn, Fe, Co, Zn and Cd).[39, 71] This connectivity of net reminds that in Hofmann clathrates and related compounds[72, 73] such as Na$_2$Cu[Fe(CN)$_6$].10H$_2$O. The main difference between the two structures originate from the smaller 2- charge of [Mo$_6$Br$_8$(CN)$_6$]$^{2-}$ than the 4- one of the [Re$_6$S$_8$(CN)$_6$]$^{4-}$. Consequently, the [*trans*-M(H$_2$O)$_2$][Mo$_6$Br$_8$(CN)$_6$] framework is neutral. The absence of large Cs$^+$ leads to the formation of hollow tubular channels along the *b* direction containing cavities of about 75 Å^3 for **1** (Fig. 4) while they are 80 Å^3 in [*trans*-Cd(H$_2$O)$_2$][Mo$_6$Br$_8$(CN)$_6$].
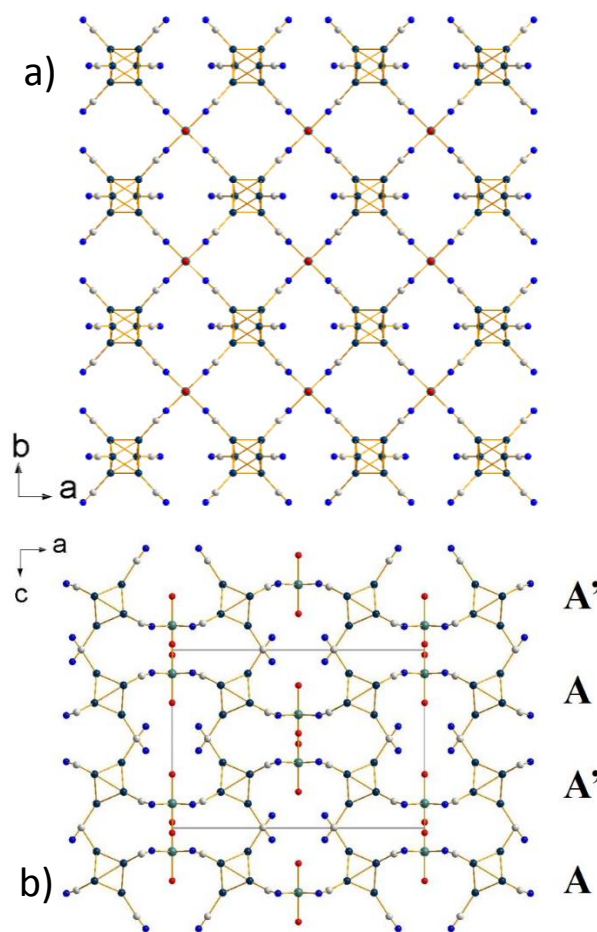
Fig. 3 a) Projection along the *c* direction of a square-net-layer in the structure of **1**. b) Projection along the *b* axis showing the AA'AA' stacking type of the square-net-layers evidencing the shift of *a*/2 between each layer. Bromine ligands have been omitted for sake of clarity.

Beyond ionic interactions between [*trans*-Mn(H$_2$O)$_2$]$^{2+}$ complexes and [Mo$_6$Br$^i_8$(CN)$^a_6$]$^{2-}$ cluster units, the structural cohesion is ensured by Br3-Br3 van der Waals interactions, hydrogen bonding between water molecules and bromines (O2-Br1 = 3.6451(1) Å (×2); O2-Br3 = 3.6885(1) Å (×2)) and between C1N1 and water molecules (N1-O1 = 2.7485(1) Å).
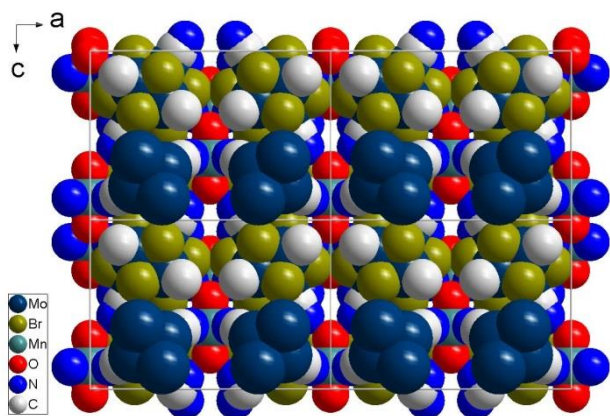
Fig. 4. Space filling model of the projection of the crystal structure of **1** in the (*a*, *c*) plane evidencing the channels parallel to the *b* axis.

Crystal structures of 2 and 3.

As **1**, **2** and **3** crystallize in the orthorhombic system, *Imma* space group (n°74) with refined unit-cell parameters a = 19.5490(8) Å, b = 10.3084(4) Å, c = 13.7398(5) Å, V = 2768.8(2) Å³ for **2** and a = 19.616(1) Å, b = 10.2909(7) Å, c = 13.8615(8) Å, V = 2798.2(3) Å³ for **3**. Atomic coordinates, relevant selected bond lengths and angles are listed in Tables S2A and S2B.
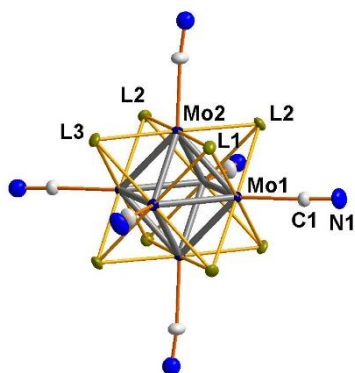

Fig. 5 Representation of the $[Mo_6Br^i_6S^i_2(CN)^a_6]^{3-}$ cluster unit in **2**.

For both compounds, Mo2, C2 and N2 fully occupy general 16*j* Wyckoff positions. Mo1, C1 and N1 fully occupy 8*i* (x, ¼, z) Wyckoff positions with C_s symmetry and Mn and O1 fully occupy 4*e* (0, ¼, z) Wyckoff positions with C_{2v} symmetry (Table S2). For **2**, O2 is located on a 8*h* (0, ¼, z) Wyckoff position with a half occupation factor and Cs1 occupies a 8*h* (0, y, z) Wyckoff position with a C_s symmetry and a refined occupation factor of roughly 34%. The face-capping Wyckoff positions (16*j* and 8*i*) are randomly occupied by Br and S as discussed below. For **3**, O2 fully occupy a 4*e* (0, ¼, z) Wyckoff position and the Cs1 refined occupation factor is roughly 41%. The face capping Wyckoff positions (16*j* and 8*i*) are randomly occupied by Br (75%) and Se (25%) as discussed below (Table S2B). **2** and **3** compounds are respectively built up from $[Mo_6Br^i_6S^i_2(CN)^a_6]^{3-}$ and $[Mo_6Br^i_6Se^i_2(CN)^a_6]^{3-}$ cluster units where the face-capping positions of the octahedral cluster are randomly occupied by six bromines and two sulfur or two selenium atoms. The six apical positions are fully occupied by cyanide ligands (C1N1 and C2N2) as depicted in Fig. 5. For **2**, the structural refinement clearly indicates that the sulfur atoms are mainly localized in the 8*i* (x, ¼, z) position (i.e. Br1/S1) and the Br/S ratio on this position is close to one. Hence, we decided to fix the Br1/S1 ratio at 1 for this position. In order to reach a Br/S composition of 6/2 equal to that found in the starting precursor for the whole cluster unit and agreeing with that deduced from the chemical analyses, the Br2/S2 and Br3/S3 ratios were then fixed to 83/17. Previous theoretical studies showed that isomer with two chalcogens around the Mo_6 octahedron where the sulfur atoms cap opposite triangular faces of the metallic octahedron is mostly present compared to the two possible others. Indeed, density functional theory (DFT) calculations on isolated $[Mo_6I^i_6Se^i_2I^a_6]^{n-}$ clusters demonstrated that this isomer is more stable than the two others both for 23 (n = 3) and 24 (n = 4) VEC species.[74] Another first-principles study devoted to $[Re_6S^i_6Br^i_2Br^a_6]^{2-}$ showed that energy differences between isomers can be tiny. This is consistent with the co-existence of all three isomers in the structure of **2**, definitely in different ratios. Mismatch between symmetry of anion in crystal structure and local symmetry of geometric isomers of $[Mo_6Br^i_6S^i_2(CN)^a_6]$ anions[75] did not allow to choose preferential isomer but their orientation in structure favours in preferential occupation of sulfur in "opposite" sites. Relatively short non-covalent L1 - L1 contacts from different anions (3.471 Å) are consistent with higher sulfur content in L1 position. Similar close contacts between highly charged ions were earlier discussed (see e.g.[76]). For **3**, the presence of both bromine and selenium elements could not be distinguished by X-ray diffraction analyses but has been clearly observed and quantified by EDS analyses. Hence, the value of the Br/Se ratio was fixed at 3 on the 16*j* (x, y, z)) and the two 8*i* (x, ¼, z) Wyckoff positions during the refinement according to chemical analyses. Similar methodology was used for the structural refinement of $Cs_4[Mo_6Br^i_6Se^i_2Br^a_6]$.[75] Note that in **3**, relatively short non-covalent L3 − L3 contacts from different anions (3.475 Å) were found similarly to those in **2**. This suggests that Se atoms are probably preferentially located on a 8*i* Br3/Se3 position. For both compounds, the average Mo-Mo distances are 2.6348(4) and 2.6459(4) Å in **2** and **3**, respectively. The Mo-L (L = Br/Q) distances range from 2.5656(7) to 2.6059(3) Å in **2** and from 2.5821(9) to 2.6084(6) Å in **3** (Table S2B). In both compounds the anionic charge of $[Mo_6Br^i_6Q^i_2(CN)^a_6]^{3-}$ (Q = S, Se) cluster units is compensated by one Mn cation according to chemical analyses but the content of the Cs^+ cations depends on the nature of the chalcogen and is refined to 0.680(4) and 0.820(4) per formula unit for **2** and **3**, respectively. To balance the charge, it requires that a part of Mn^{II} was oxidized in Mn^{III} and the content of the Cs^+ is directly related to that of Mn^{II}. Consequently, the final formula must be written after final refinements $Cs_{0.680(4)}[trans-(Mn^{II}_{0.680(4)}Mn^{III}_{0.320(4)})(H_2O)_2]-[Mo_6Br^i_6S^i_2(CN)^a_6]$ and $Cs_{0.820(4)}[trans-(Mn^{II}_{0.820(4)}Mn^{III}_{0.180(4)})(H_2O)_2][Mo_6Br^i_6Se^i_2(CN)^a_6]$ for **2** and **3**, respectively. Bond lengths comparison between **2**, **3**, **4** and **5** (*i.e.* $[Mo_6Br^i_6Q^i_2(CN)^a_6]$ cluster units based compounds) as well magnetic properties, luminescent measurements and theoretical calculations will be discussed below. They

unambiguously show that **2** and **3** are based on $[Mo_6Br^i_6Q^i_2(CN)^a_6]^{3-}$ cluster units with a VEC = 23. One can remind that oxidation potential of $[Mo_6Br^i_6Q^i_2(CN)^a_6]^{4-}$ was reported to be $E_{1/2}$ = -0.056 V and -0.068 V (vs ECS in acetonitrile) for Q = S and Se, respectively. Consequently, oxidation of $[Mo_6Br^i_6Q^i_2(CN)^a_6]^{4-}$ chalcohalides is easier to obtain than oxidation of pure bromides ($E_{1/2}$ = + 1.38 V).[19] The structures of **2** and **3** are strongly related to that of **1**. Indeed, they crystallize in the same space group with similar unit cell parameters (Table 1) and the structures are all described as 2D extended polymeric square-net-layers stacked along c according axis to a AA'AA' arrangement. The cluster building block is the diamagnetic $[Mo_6Br^i_8(CN)^a_6]^{2-}$ cluster unit for **1** and the magnetic $[Mo_6Br^i_6Q^i_2(CN)^a_6]^{3-}$ one for **2** and **3**. For the latter ones, the anionic charge (n-) of $[trans-(Mn^{II}_xMn^{III}_{1-x})(H_2O)_2][Mo_6Br_6Q_2(CN)_6]^{n-}$ (Q = S, Se) square-net-layers is counterbalanced by the presence of x Cs$^+$ (n = x) cations which are located in the channels as depicted in Fig. 6.
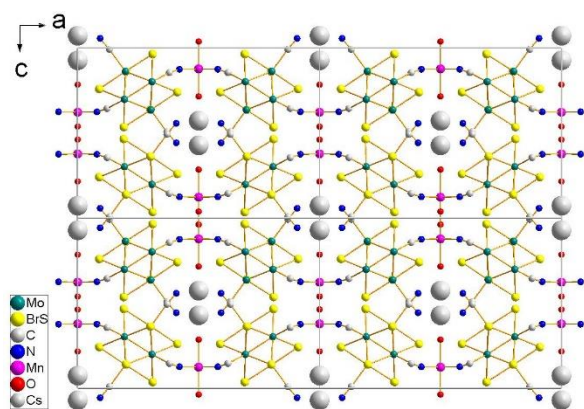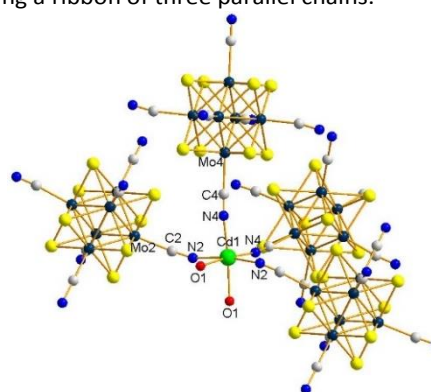

Fig. 6 Projection along the *b* direction of the crystal structure of **2** evidencing the presence of the Cs$^+$ cations in the channels.

As **1**, the structures of **2** and **3** are also strongly related to that of $Cs_2[trans-M(H_2O)_2][Re_6S^i_8(CN)^a_6]$ (M = Mn, Fe, Co, Zn and Cd).[39, 71] Indeed the cluster units and the $[trans-M(H_2O)_2]$ moieties form similar arrangement but in the $[Re_6S^i_8(CN)^a_6]^{4-}$ based compounds, there are two Cs$^+$ per formula to counter balance the 4- charge. They are located in the channels for one half (4e Wyckoff position) and for the other half, they are centred in half of the holes in the two dimensional net (4d Wyckoff position) structurally related to that shown in Fig. 3a. In **2** and **3**, based on $[Mo_6Br^i_6Q^i_2(CN)^a_6]^{3-}$ oxidized clusters, Cs$^+$ are only located in the channels (Fig. 6) and the x content is directly related to that of Mn^{II}.
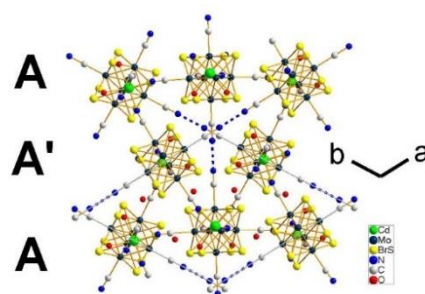
Crystal structures of 4 and 5.

4 and **5** compounds crystallize in the trigonal system in the non centro-symmetric $P3_121$ space group (n°152) with refined unit cell parameters a = 13.2013(6) Å, c = 14.1296(6) Å, V = 2132.5(2) Å^3 for **4** and a = 13.2807(5) Å, c = 14.1753(6) Å, V = 2165.2(2) Å^3 for **5**. Atomic coordinates, relevant selected bond lengths and angles are listed in Tables S3A and S3B. For both compounds, Mo2, Mo4, C2, N2, C4, N4, O1 and O2 fully occupy general 6c Wyckoff positions while Mo1, Mo3, C1, C3, N1 and N3 fully

occupy 3b (x, x, ½) Wyckoff positions with C_2 symmetry. Cd1 fully occupies a 3a (0, y, 2/3) Wyckoff position with C_2 symmetry. Face-capping positions (6c) are randomly occupied by Br (75%) and S (25%) for **4** and by Br (75%) and Se (25%) for **5**. **4** and **5** are respectively built up from $[Mo_6Br^i_6S^i_2(CN)^a_6]^{4-}$ and $[Mo_6Br^i_6Se^i_2(CN)^a_6]^{4-}$ cluster units where the face-capping positions of the octahedral cluster are randomly occupied by six bromine and two sulfur or two selenium atoms. The six apical positions are fully occupied by cyanide ligands. Mismatch between symmetry of anion in crystal structure of **4** and local symmetry of geometric isomers of $[Mo_6Br^i_6S^i_2(CN)^a_6]$ anions[75] did not allow to refine correctly the Br:S ratio. For **5**, the presence of both bromine and selenium elements could not be distinguished by X-ray diffraction analyses. For both compounds the value of the Br/Q (Q = S, Se) ratio was then fixed at 0.75:0.25 during the refinement according to chemical analyses and a previous structural refinement on $Cs_4[Mo_6Br^i_6Q^i_2Br^a_6]$.[75] The average Mo-Mo distances are 2.627(2) and 2.637(2) Å in **4** and **5**, respectively (Table 3B). The Mo-L (L = Br/Q) distances range from 2.577(3) to 2.600(4) Å in **4** and from 2.588(3) to 2.603(2) Å in **5**. These distances are within the range observed in $Cs_{0.5}K_{0.5}(Et_4N)_{11}[Mo_6Br_6Q_2(CN)_6]_3$ (Q = S, Se)[75] which are built up from the same $[Mo_6Br^i_6Q^i_2(CN)^a_6]^{4-}$ (Q = S, Se) cluster units. In **4** and **5**, as for **1**, the metal is coordinated by four CN groups belonging to the $[Mo_6Br^i_6Q^i_2(CN)^a_6]^{4-}$ cluster units and two water molecules but, in **4** and **5**, the two water molecules are in *cis* position (Fig. 7). In the crystal structure of both compounds the $[Mo_6Br^i_6Q^i_2(CN)^a_6]^{4-}$ cluster units are stacked along the [110] direction following a AA'A stacking type (Fig. 8). As depicted on Fig. 9, each cluster anionic unit is surrounded by four [*cis*-Cd(H_2O)_2]$^{2+}$ cations. Within the A layer, the $[Mo_6Br^i_6Q^i_2(CN)^a_6]^{4-}$ anions and [*cis*-Cd(H_2O)_2]$^{2+}$ cations build chains along the *c* direction. The former ones are connected one to each other by [*cis*-Cd(H_2O)_2]$^{2+}$ cations of adjacent chains *via* Mo4-C4-N4-Cd2 bonds forming a ribbon of three parallel chains.

Fig. 7 Representation of the cadmium environment in **4** evidencing the *cis* position of the water molecules.

Fig. 8 Projection along the c axis of the crystal structure of **4** evidencing the AA'A stacking type. Blue dashed lines correspond to CN H⁺-NC bridges.
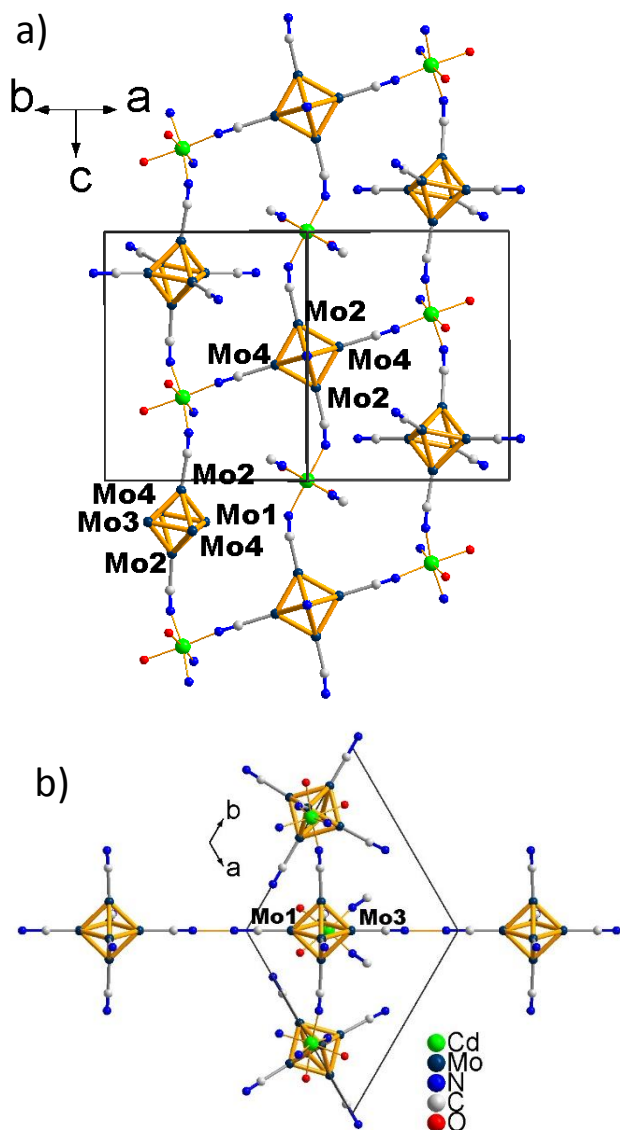
Fig. 9 a) Projection of A layer along [110] direction in **4** evidencing connections of the central cluster unit. b) Projection of A layer along the *c* axis in **4** evidencing a linear chain of $[Mo_6Br^i_6S^i_2(CN)^a_6]^{4-}$ cluster units interconnected by H⁺ that spreads along the [110] direction.

The anionic charge of the $\{[cis\text{-}Cd(H_2O)_2][Mo_6Br^i_6Q^i_2(CN)^a_6]\}^{2-}$ framework must be compensated by a +2 charge. Chemical analyses do not reveal the presence of heaviest elements than those used in the structural refinement. Hence, the two single charges must be provided by H⁺ protons. It could be H⁺ protonating the H_2O molecules located between the layers and in the cavities of the layers. But owing to rather short N1-N3 interatomic distances (3.0348(1) Å and 3.0089(1) Å for **4** and **5**, respectively), it can be assumed that one H⁺ could be located between C1N1 and C2N2. This assumption is supported by the fact that the crystal structures of **4** and **5** are related to that of H[cis-Fe(H₂O)₂][Re₆Se₈(CN)₆]-2H₂O.[39] For the latter, the distance

N-N is very short owing to the presence of one H⁺ between the nitrogen atoms 2.50(3) Å that reflects the strength of the hydrogen bonding in the N-H•••N bridges.[39] Despite longer in **4** and **5** than in H[cis-Fe(H₂O)₂][Re₆Se₈(CN)₆]-2H₂O, the N-N distance is however shorter than similar distances usually reported for compounds containing CN⁻-⁻NC contacts (around 3.5 Å). The C1N1 and C3N3 lie in *trans* position around the cluster units. As a consequence, the association of cluster units *via* H⁺ protons (one H⁺ per cluster unit) enables the formation of infinite chains Mo₆-C1N1-H-N3C3-Mo₆-C1N1-H-. These chains sketched in Fig. 9 are perpendicular to the ribbon described above. On the other hand, the second H⁺ must statistically protonate one of the two equivalent positions of the water molecules leading to the formula: (H₃O)H[cis-Cd(H₂O)₂][Mo₆Br^i₆Q^i₂(CN)^a₆]-H₂O. Beyond interactions within the chains (*i.e.* coordination bonds between anion and cations along with hydrogen bonding involving CN groups of adjacent cluster), the structural cohesion of **4** and **5** is ensured by Br1-Br3 van der Waals (Fig.S2 ESI) contacts and hydrogen bonding involving H₃O⁺ and water molecules, (O2-O1 = 2.7217(1) Å, O2-N2 = 3.3611(2) Å, O2-Br2 = 3.5636(1) Å and L1-L3 = 3.5530(1) Å for **4**; O2-O1 = 2.7756(1) Å, O2-N2 = 3.3123(1) Å, O2-Br2 = 3.6389(1) Å and L1-L3 = 3.5843(1) Å for **5**).

Evolution of bond distances and theoretical considerations

The anionic charge of the $\{[cis\text{-}Cd(H_2O)_2][Mo_6Br^i_6Q^i_2(CN)^a_6]\}^{2-}$ framework is compensated by the presence of two H⁺ counter-cations in **4** and **5** leading to the most stable electronic configuration (VEC = 24). It is well known that moving from a VEC of 24 to a VEC of 23 requires to remove an electron of the predominant metal-metal binding orbitals which implies a weakening of the Mo-Mo distance and to a lesser extent, a weakening of the Mo-L distances.[27] Consequently, if **2** and **3** are based on $[Mo_6Br^i_6Q^i_2(CN)^a_6]^{3-}$ cluster units, they must exhibit Mo-Mo and Mo-L distances longer than those found in **4** and **5**. Analysis of bond lengths from Table 2 shows that Mo-L^i distances are similar in **2**, **3**, **4** and **5** but Mo-Mo and Mo-L^a distances are significantly longer in **2** than in **4** (Q = S) and significantly longer in **3** than in **5** (Q = Se). This unambiguously proves that **2** and **3** are based on cluster units with a VEC of 23. Moreover, if the Mn^II cations are partially oxidized in **2** and **3**, the Mn-N distances should be shorter in **2** and **3** than in **1** which is shown again in Table 2.

Table 2 Comparison of the Mo-Mo and Mo-L distances between **2**, **3**, **4** and **5** and comparison of the Mn-N et Mn-O distances between 1 and 3.

Compound	1	2	3	4	5
VEC	24	23	23	24	24
Mo-Mo (Å)	2.633(2)	2.6267(4)	2.638(1)	2.624(2)	2.634(2)
	2.635(1)	2.6348(4)	2.6459(4)	2.626(2)	2.636(2)
	2.636(1)	2.6484(4)	2.6528(6)	2.632(2)	2.642(2)
Mo-L^i (Å)	2.586(2)	2.5654(7)	2.5820(9)	2.577(3)	2.588(2)
	2.592(2)	2.5933(5)	2.6004(6)	2.591(3)	2.597(2)
	2.596(2)	2.6060(4)	2.6084(6)	2.602(3)	2.603(2)
Mo-C (Å)	2.18(2)	2.195(5)	2.195(7)	2.150(3)	2.179(3)
Mn-N (Å)	2.22(1)	2.191(2)	2.188(5)		
Mn-O (Å)	2.265(2)	2.237(7)	2.242(9)		

Table 3 Main averaged optimized distances in Cs$_x$[*trans*-Mn(H$_2$O)$_2$]-[Mo$_6$Br$^i_6$S$^i_2$(CN)$^a_6$] (x = 0.5, 1) models.

Contacts	x = 0.5	x = 1
Mo-Mo (Å)	2.673	2.663
Mo-S^i (Å)	2.416	2.422
Mo-Br^i (Å)	2.623	2.631
Mo-C (Å)	2.161	2.144
Mn-N (Å)	1.943	1.949
Mn-O (Å)	1.981	2.276

To gain further insight on the charge distributions over transition metal and cluster units in **2** and **3**, periodic DFT calculations were carried out. Since capping positions can be occupied by a chalcogen or bromine, a model compound based on the crystal structure of **2** has been considered. In this model, the sulfur atoms lie on Br1/S1 position whereas other triangular faces are capped mainly by Br in agreement with the relative occupation numbers. Different contents of caesium have been considered, corresponding to the formula Cs$_x$[*trans*-Mn(H$_2$O)$_2$]-[Mo$_6$Br$^i_6$S$^i_2$(CN)$^a_6$] (x = 0.5, 1), as well as different magnetic configurations. Cell parameters and atomic positions were free to relax; main distances are reported in Table 3. All computed formula and magnetic configurations exhibit band structures (not shown here) characterized by flat bands, indicating that very few interactions occur between motifs in the structure. This is consistent with the low dimensional character of the structures of all compounds described in this work. Whatever the content of caesium (x = 0.5, 1), models with high-spin state configuration for Mn are largely preferred with respect to energy. In the case of Cs$_{0.5}$[*trans*-Mn(H$_2$O)$_2$]-[Mo$_6$Br$^i_6$S$^i_2$(CN)$^a_6$], two scenarios of charge distribution can be envisioned; both assume an electron transfer from the alkaline metal towards the more electronegative atoms of the compound. Either an equal mix of Mn^{II}/Mn^{III} ions are present with 23-VEC clusters, or

only Mn^{II} are present with an equal mix of 22- and 23-VEC species. Owing to the significant lower stability of 22-VEC clusters,[77] the second scenario is much less believable than the first one. In the case of Cs[*trans*-Mn(H$_2$O)$_2$]-[Mo$_6$Br$^i_6$S$^i_2$(CN)$^a_6$], two scenarios of charge distribution can also be envisioned: one considers the presence of Mn^{II} and 23-VEC clusters, the other one consists in the presence of an equal mix of Mn^{II} and Mn^{III} with an equal mix of 23- and 24-VEC clusters. Optimized distances in Cs$_x$[*trans*-Mn(H$_2$O)$_2$]-[Mo$_6$Br$^i_6$S$^i_2$(CN)$^a_6$] (x = 0.5, 1) models can help in identifying which charge distribution is favoured. The optimized distances are hardly perturbed by the content of caesium in the structure, except Mn-O that much increases in the case of Cs[*trans*-Mn(H$_2$O)$_2$]-[Mo$_6$Br$^i_6$S$^i_2$(CN)$^a_6$]. Such a large increase can be attributed to the change of the oxidation state of Mn: for Mn^{II}, two electrons lie in M-L* orbitals compared to only one in the case of Mn^{III}. Therefore the antibonding character is reinforced leading to a substantial lengthening of Mn-O distances in Cs[*trans*-Mn(H$_2$O)$_2$]-[Mo$_6$Br$^i_6$S$^i_2$(CN)$^a_6$]. These theoretical results support the presence of 23-VEC clusters in compounds **2** and **3**, whatever the content of caesium in the structure.

Optical properties.

1-5 being insoluble compounds, optical properties measurements were performed on powder. The shape of reflectance spectra of **1-5** (ESI Fig. S6-S9) typically corresponds to that of semiconducting compounds. **1-5** absorb continuously from UV to vis. Positions of band maxima were obtained graphically from spectra reported in ESI. **1** exhibits only one absorption band maxima located at 540 nm whilst those of **2-5** exhibit two band maxima. **1**, **4** and **5** are built up from Mo$_6$ clusters with a valence concentration of 24. The first band maxima of **4** and **5** is located at 535 nm and 550 nm respectively. It indicates that the substitution of two Br by two S atoms induces a blue shift of the absorption and that the substitution of two Br by two Se atoms induces the opposite effect with a red shift. The second absorption maxima of **4** and **5** is located roughly at the same position around 412 nm. Comparing the spectra of **4** and **2** enables to evidence the effect of the one electron oxidation of [Mo$_6$Br$^i_6$S$^i_2$(CN)$^a_6$]$^{4-}$ to [Mo$_6$Br$^i_6$S$^i_2$(CN)$^a_6$]$^{3-}$. Going from **4** to **2** induces a shift of the band maxima from 535 and 412 nm to 540 and 400 nm respectively. Comparing spectra of **5** and **3** enables to evidence the effect of the one electron oxidation of [Mo$_6$Br$^i_6$Se$^i_2$(CN)$^a_6$]$^{4-}$ to [Mo$_6$Br$^i_6$Se$^i_2$(CN)$^a_6$]$^{3-}$. Going from **5** to **3** induces a shift of the band maxima from 550 and 412 nm to 544 and 410 nm respectively.

It is well known that octahedral Mo$_6$ cluster units with a VEC equal to 24 exhibit luminescent properties whereas no emission properties are expected for oxidized 23-VEC species.[78] Typically, such compounds with a VEC of 24 exhibit a continuous and larger emission window from UV to vis and a large emission widow from vis to near infra-red region. It is known that the most efficient excitation is obtained in the UV/blue region.[13, 14]

As **2** and **3** are based on $[Mo_6Br^i_6Q^i_2(CN)^a_6]^{3-}$ cluster units (VEC = 23), they are not supposed to emit while **4** and **5** should exhibit luminescent properties. Fig. 10 displays the luminescent spectra at 93K for **2**, **3**, **4** and **5** recorded on crystalline powder using excitation wavelength bandwidth of 350-380 nm. It clearly evidences that **4** and **5** are luminescent while **2** and **3** are not. This which constitutes another evidence for the presence of 23 VEC species in the compounds **2** and **3**. The shapes of emission spectra are typical of molecular compounds based on $[Mo_6X^i_8L^a]$ cluster units with VEC = 24.[13,14] Emission maxima are found at around 675 nm for both **4** and **5**.
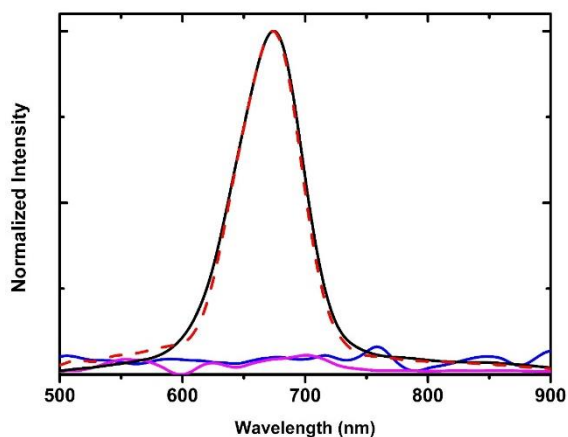

Fig. 10 Luminescence spectra of sample **2** (blue), **3** (magenta), **4** (black) and **5** (dashed red) in crystalline powder form measured at 93K with an excitation wavelength bandwidth of 330-380 nm.

Oxidation of manganese in 2 and 3 and magnetic properties.

First, the coexistence of the two oxidation states Mn^{2+} and Mn^{3+} in **2** and **3** was evidenced by electron energy loss spectroscopy experiments. Figure 11 displays the manganese $L_{2,3}$ edges spectra of the three commercial oxides and compounds **2** and **3**. The spectra of pure Mn^{2+} and Mn^{3+} oxides are quite similar to previous studies and show that (i) the L3 peak shift to higher energy as the valency of manganese is increased, (ii) the ratio of integrated L3 and L2 peaks is correlated to this valency. [79-81] Spectrum of Mn^{2+}/Mn^{3+} oxide (Mn_3O_4) is also similar to the results published by Laffont and Gibot.[79] These authors showed that the mixed valence in Mn_3O_4 gives rise to 2 peaks for L3 edge, one for Mn^{2+} and the second one for Mn^{3+}. Spectra of compounds **2** and **3** present similar features to that of Mn_3O_4 spectrum, evidencing the presence of both valancies in these materials. The height of Mn^{3+} L3 peak is lower than that of the corresponding peak observed for Mn_3O_4, indicating that the ratio Mn^{3+}/Mn^{2+} is far below 2. Second, magnetic measurements were performed for compounds **2** and **3**; Fig. 12 displays the temperature dependence of their magnetic susceptibility. The magnetic susceptibility data are well described by the Curie-Weiss Law, $\chi = \chi_o + C/(T-\Theta_p)$ where χ is the magnetic susceptibility, C, the Curie constant and Θ_p, the paramagnetic Curie temperature. Least-squares fitting of these data leads to $\chi_o = 0.0013(2)$ emu mol^{-1}, C = 4.319(5) emu K mol^{-1}

Θ_p = -0.189(3) K and $\chi_o = 0.0033(3)$ emu mol^{-1}, C = 4.467(7) emu K mol^{-1}, Θ_p = -0.210(5) K for **2** and **3**, respectively. Since $\mu_{eff} \sim (8C)^{1/2}$, the effective magnetic moment is equal to 5.88(5) μ_B and 5.98(7) μ_B for **2** and **3**, respectively.
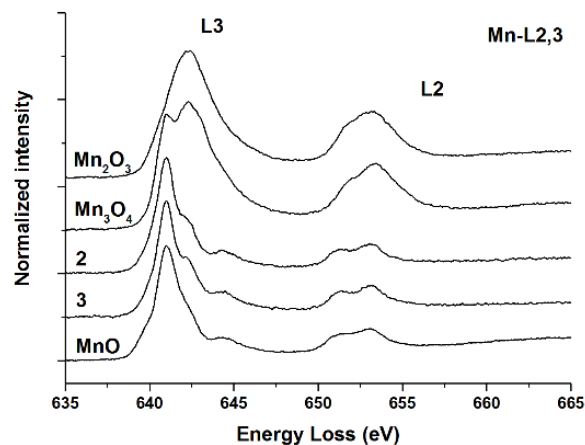
Fig. 11 Manganese L2,3 edge of MnO, Mn_3O_4, Mn_2O_3 oxides and compounds **2** and **3**, after background subtraction.
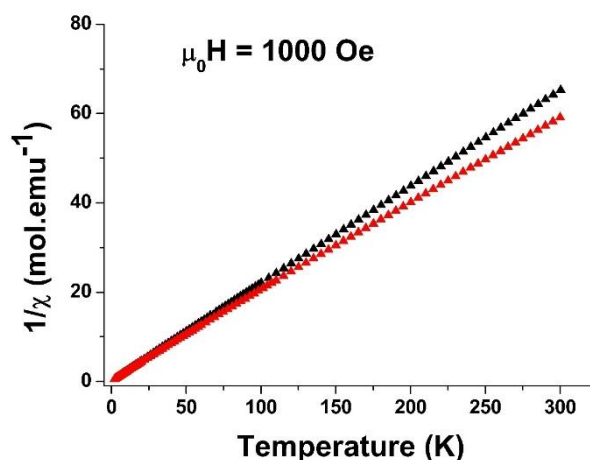
Fig. 12 Temperature dependence of the inverse magnetic susceptibility for **2** (black) and **3** (red).

Table S4 summarizes the values of Curie constants for each possible configuration for Mn cations and cluster unit in **2** and **3** (*i.e.* Mn^{II} in high or low spin environment; Mn^{III} in high or low spin environment and a paramagnetic cluster with one unpaired electron (VEC = 23) or a diamagnetic cluster (VEC = 24)). Table S5 summarizes the sum of Curie constant calculated taking into account all the possible combination between Mn$^{II/III}$ low or high spin with diamagnetic or paramagnetic cluster. The experimental Curie constant values deduced from magnetic measurements are 4.319(5) and 4.467(7) emu K mol^{-1} for **2** and

3, respectively. This corresponds to the theoretical values obtained considering Mn^{II} and Mn^{III} cations in high spin environment and a paramagnetic cluster (*i.e.* H column in Table S5: C = 4.31 emu K mol^{-1} and C = 4.5025 emu K mol^{-1} for **2** and **3**, respectively). From experimental Curie constant, the effective magnetic moments are calculated to be 5.88(5) μ_B and 5.98(7) μ_B. These values match very well with theoretical ones (5.87 μ_B and 6.00 μ_B for **2** and **3**, respectively). In both compounds, no magnetic coupling was evidenced.

4. Discussion and conclusion.

The present work constitutes the first deep investigations of crystal structures and physical properties combined with theoretical rationalization of low dimensional compounds based on Mo_6 cyanides. If, Re_6 cyanides with face-capping chalcogen ligands and Nb_6 cyanides with edge-bridged halogen ligands have been widely used as building blocks in the design of coordination polymers with different dimensionalities, ~~but~~ it turns out that very few is known about Mo_6 cyanides chemistry and structures. Mo_6 clusters can be face-capped by halogen, chalcogen or a mixture of both. Octahedral cluster cyano complexes are obtained in face-capped units $[Re_6Q^i_8(CN)^a_6]^{m-}$ (Q = chalcogen) as well as in edge-bridged units $[Nb_6X^i_{12}(CN)^a_6]^{n-}$ (X = halogen). In general, Re_6 and Nb_6 cyanides demonstrate geometric rigidity and stability in wide range of experimental conditions and, meanwhile, have larger size and greater ability to one- and multi-electron redox transformations than mononuclear cyanide complexes. Prussian Blue structural type with NaCl packing realizes not only for $[Re_6Se_8(CN)_6]$ with the charge 3- [39], but also for highly charged $[Nb_6Cl_{12}(CN)_6]^{4-}$ [82] $[Re_3Mo_3S_8(CN)_6]^{6-}$ [83] and $[Mo_6Se_8(CN)_6]^{7-}$ [84] with various cations compensating negative charge of framework. The analysis of Table S6 evidences that Mo_6 cluster units despite their differences with Re_6 and Nb_6 ones (atomic composition, electronic structures, VEC numbers) have similar dimensions and topologies. Consequently, it favours the formation of common structural types and structures as illustrated by the new compounds **1-5**. Layered structures **1–3** with connectivity 4:4 are structurally related to those found in $Cs_2[trans-M(H_2O)_2][Re_6S_8(CN)_6]$ (M = Mn, Fe, Co, Zn and Cd) [39, 71] and remind $(NMe_4)_2[Mn(H_2O)_4][Fe(CN)_6]\cdot4H_2O$ and Hofmann clathrates.[73] The charge of the framework (0 for **1**; −2 for $Cs_2[trans-M(H_2O)_2][Re_6S_8(CN)_6]$; -0.68 and -0.82 for **2**, **3** respectively) is compensated by counter-cations located in cavities of the framework. Similarly, compounds **4** and **5** are structurally related to $H[cis-Fe(H_2O)_2][Re_6Se_8(CN)_6]\cdot2H_2O$[39] crystallizing in chiral $P3_121$ space group with close metric of unit cell. Structures of $[trans-Cd(H_2O)_2]-[Mo_6Br_8(CN)_6]$,[51] **1, 2** and **3** are strongly related one to each other but are very different to that of **4** and **5** $((H_3O)H[cis-Cd(H_2O)_2][Mo_6Br^i_6Q^i_2(CN)^a_6]-H_2O)$. It is worth noting that cavities occupied with Cs^+ cations in **2** and **3** could have hosted 2 H_3O^+ as found in $Cs_2[trans-M(H_2O)_2][Re_6S_8(CN)_6]$.[39, 71] Instead, an important structural evolution is observed: the cadmium environment changes from *trans* to *cis* configurations and chains of clusters are formed by

the presence of one H^+ between 1/3 of CN groups of cluster units. To sum up, this work reports new compounds based on $[Mo_6Br^i_8(CN)^a_6]^{2-}$ and $[Mo_6Br^i_6Q^i_2(CN)^a_6]^{n-}$ (Q = S, Se; n=3, 4) cluster units. Existence of stable structural types for such hexacyano building blocks differently charged open the way for materials with tuned charge of framework and controlled properties. For instance, concerning the $[Mo_6Br^i_6Q^i_2(CN)^a_6]^{n-}$: for a 4- charge, the cluster is diamagnetic and luminescent and for a 3- charge, the cluster is paramagnetic and do not exhibit any luminescence properties. Such modulation of optical and magnetic properties by charge switching is particularly relevant for the elaboration of functional hybrid materials.[14]

Conflicts of interest

There are no conflicts to declare.

Notes and references

1. H. Schäfer, H. G. V. Schnering, J. Tillack, F. Kuhnen, H. Wöhrle and H. Baumann, *Z. Anorg. Allg. Chem.*, 1967, **353**, 281-310.
2. M. Potel, C. Perrin, A. Perrin and M. Sergent, *Mater. Res. Bull.*, 1986, **21**, 1239-1245.
3. G. Pilet and A. Perrin, *Solid State Sci.*, 2004, **6**, 109-116.
4. K. Kirakci, S. Cordier and C. Perrin, *Z. Anorg. Allg. Chem.*, 2005, **631**, 411-416.
5. K. Kirakci, S. Cordier, O. Hernandez, T. Roisnel, F. Paul and C. Perrin, *J. Solid State Chem.*, 2005, **178**, 3117-3129.
6. M. W. Willer, J. R. Long, C. C. McLauchlan and R. H. Holm, *Inorg. Chem.*, 1998, **37**, 328-333.
7. B. K. Roland, W. H. Flora, M. D. Carducci, N. R. Armstrong and Z. Zheng, *J. Clust. Sci.*, 2003, **14**, 449-458.
8. K. Kirakci, H. Hosoda, S. Cordier, C. Perrin and G. Saito, *J. Solid State Chem.*, 2006, **179**, 3628-3635.
9. S. Cordier, Y. Molard, K. A. Brylev, Y. V. Mironov, F. Grasset, B. Fabre and N. G. Naumov, *J. Clust. Sci.*, 2015, **26**, 53-81.
10. A. W. Maverick, J. S. Najdzionek, D. MacKenzie, D. G. Nocera and H. B. Gray, *J. Am. Chem. Soc.*, 1983, **105**, 1878-1882.

11.   T. G. Gray, C. M. Rudzinski, D. G. Nocera and R. H. Holm, *Inorg. Chem.*, 1999, **38**, 5932+.
12.   T. G. Gray, C. M. Rudzinski, E. E. Meyer, R. H. Holm and D. G. Nocera, *J. Am. Chem. Soc.*, 2003, **125**, 4755-4770.
13.   K. Costuas, A. Garreau, A. Bulou, B. Fontaine, J. Cuny, R. Gautier, M. Mortier, Y. Molard, J. L. Duvail, E. Faulques and S. Cordier, *Phys. Chem. Chem. Phys.*, 2015, **17**, 28574-28585.
14.   B. Dierre, K. Costuas, N. Dumait, S. Paofai, M. Amela-Cortes, Y. Molard, F. Grasset, Y. Cho, K. Takahashi, N. Ohashi, T. Uchikoshi and S. Cordier, *Sci. Techn. Adv. Mater.*, 2017, **18**, 458-466.
15.   A. Barras, S. Cordier and R. Boukherroub, *Appl. Catal. B*, 2012, **123**, 1-8.
16.   P. Kumar, N. L. G. Naumov, R. Boukherroub and S. L. Jain, *Appl. Catal. A*, 2015, **499**, 32-38.
17.   P. Kumar, S. Kumar, S. Cordier, S. Paofai, R. Boukherroub and S. L. Jain, *RSC Adv.*, 2014, **4**, 10420-10423.
18.   S. Kumar, O. P. Khatri, S. Cordier, R. Boukherroub and S. L. Jain, *Chem. Eur. J.*, 2015, **21**, 3488-3494.
19.   J. A. Jackson, C. Turro, M. D. Newsham and D. G. Nocera, *J. Phys. Chem.*, 1990, **94**, 4500-4507.
20.   K. Kirakci, P. Kubat, M. Dusek, K. Fejfarova, V. Sicha, J. Mosinger and K. Lang, *Eur.J. Inorg. Chem.*, 2012, 2, 3107-3111.
21.   K. Kirakci, P. Kubat, J. Langmaier, T. Polivka, M. Fuciman, K. Fejfarova and K. Lang, *Dalton Trans.*, 2013, **42**, 7224-7232.
22.   K. Kirakci, V. Sicha, J. Holub, P. Kubat and K. Lang, *Inorg. Chem.*, 2014, **53**, 13012-13018.
23.   K. Kirakci, P. Kubat, K. Fejfarova, J. Martincik, M. Nikl and K. Lang, *Inorg. Chem.*, 2016, **55**, 803-809.
24.   Y. Molard, C. Labbe, J. Cardin and S. Cordier, *Adv. Funct. Mater.*, 2013, **23**, 4821-4825.
25.   M. N. Sokolov, M. A. Mihailov, E. V. Peresypkina, K. A. Brylev, N. Kitamura and V. P. Fedin, *Dalton Trans.*, 2011, **40**, 6375-6377.
26.   J. H. Golden, H. B. Deng, F. J. Disalvo, J. M. J. Frechet and P. M. Thompson, *Science*, 1995, **268**, 1463-1466.
27.   A. Garreau, F. Massuyeau, S. Cordier, Y. Molard, E. Gautron, P. Bertoncini, E. Faulques, J. Wery, B. Humbert, A. Bulou and J.-L. Duvail, *ACS Nano*, 2013, **7**, 2977-2987.
28.   Y. Molard, F. Dorson, V. Circu, T. Roisnel, F. Artzner and S. Cordier, *Angew. Chem. Int. Ed.*, 2010, **49**, 3351-3355.
29.   Y. Molard, A. Ledneva, M. Amela-Cortes, V. Circu, N. G. Naumov, C. Meriadec, F. Artzner and S. Cordier, *Chem. Mater.*, 2011, **23**, 5122-5130.
30.   S. K. Nayak, M. Amela-Cortes, C. Roiland, S. Cordier and Y. Molard, *Chem. Commun.*, 2015, **51**, 3774-3777.
31.   M. Prevot, M. Amela-Cortes, S. K. Manna, S. Cordier, T. Roisnel, H. Folliot, L. Dupont and Y. Molard, *J. Mater. Chem. C*, 2015, **3**, 5152-5161.
32.   M. Prevot, M. Amela-Cortes, S. K. Manna, R. Lefort, S. Cordier, H. Folliot, L. Dupont and Y. Molard, *Adv. Funct. Mater.*, 2015, **25**, 4966-4975.
33.   S. K. Nayak, M. Amela-Cortes, M. M. Neidhardt, S. Beardsworth, J. Kirres, N. Mansueto, S. Cordier, S. Laschat and Y. Molard, *Chem. Commun.*, 2016, **52**, 3127-3130.
34.   F. Grasset, F. Dorson, S. Cordier, Y. Molard, C. Perrin, A. M. Marie, T. Sasaki, H. Haneda, Y. Bando and M. Mortier, *Adv. Mater.*, 2008, **20**, 143-148.
35.   N. G. Naumov, S. Cordier and C. Perrin, *Angew. Chem. Int. Ed.*, 2002, **41**, 3002-3004.
36.   N. G. Naumov, A. V. Virovets, M. N. Sokolov, S. B. Artemkina and V. E. Fedorov, *Angew. Chem. Int. Ed.*, 1998, **37**, 1943-1945.
37.   L. G. Beauvais, M. P. Shores and J. R. Long, *Chem. Mater.*, 1998, **10**, 3783-3786.
38.   M. P. Shores, L. G. Beauvais and J. R. Long, *J. Am. Chem. Soc.*, 1999, **121**, 775-779.
39.   M. V. Bennett, L. G. Beauvais, M. P. Shores and J. R. Long, *J. Am. Chem. Soc.*, 2001, **123**, 8022-8032.
40.   Y. Kim, S.-M. Park, W. Nam and S.-J. Kim, *Chem. Commun.*, 2001, 1470-1471.
41.   Y. V. Mironov, O. Oeckler, A. Simon and V. E. Fedorov, *Eur.J. Inorg. Chem.*, 2001, 2751-2753.
42.   S. B. Artemkina, N. G. Naumov, A. V. Virovets, S. A. Gromilov, D. Fenske and V. E. Fedorov, *Inorg. Chem. Commun.*, 2001, **4**, 423-426.
43.   Y. Kim, S. M. Park and S. J. Kim, *Inorg. Chem. Commun.*, 2002, **5**, 592-595.
44.   Y. V. Mironov, O. A. Efremova, D. Y. Naumov, W. S. Sheldrick and V. E. Fedorov, *Eur.J. Inorg. Chem.*, 2003, 2591-2595.
45.   K. A. Brylev, N. G. Naumov, G. Peris, R. Llusar and V. E. Fedorov, *Polyhedron*, 2003, **22**, 3383-3387.
46.   K. A. Brylev, Y. V. Mironov, N. G. Naumov, V. E. Fedorov and J. A. Ibers, *Inorg. Chem.*, 2004, **43**, 4833-4838.
47.   K. A. Brylev, P. Sekar, N. G. Naumov, V. E. Fedorov and J. A. Ibers, *Inorg. Chim. Acta*, 2004, **357**, 728-732.
48.   N. G. Naumov, M. S. Tarasenko, A. V. Virovets, Y. Kim, S. J. Kim and V. E. Fedorov, *Eur.J. Inorg. Chem.*, 2006, 298-303.
49.   M. S. Tarasenko, E. O. Golenkov, N. G. Naumov, N. K. Moroz and V. E. Fedorov, *Chem. Commun.*, 2009, 2655-2657.
50.   M. S. Tarasenko, N. G. Naumov, D. Y. Naumov, S. J. Kim and V. E. Fedorov, *Polyhedron*, 2008, **27**, 2357-2364.
51.   M. Amela-Cortes, S. Cordier, N. G. Naumov, C. Meriadec, F. Artzner and Y. Molard, *J. Mater. Chem. C*, 2014, **2**, 9813-9823.
52.   C. Brosset, *Arkiv. Kemi, Mineral. Geol.*, 1946, **A22**.
53.   J. C. Sheldon, *J. Chem. Soc.*, 1962, DOI: 10.1039/JR9620000410, 410-415.
54.   M. Feliz, M. Puche, P. Atienzar, P. Concepcion, S. Cordier and Y. Molard, *Chemsuschem*, 2016, **9**, 1963-1971.
55.   A. Renaud, F. Grasset , B. Dierre , T. Uchikoshi, N. Ohashi , T. Takei, A. Planchat, L. Cario, S. Jobic, F. Odobel and S. Cordier, *ChemistrySelect*, 2016, **1**, 2284-2289.
56.   G. Daigre, M. S. Tarasenko, L. A. Y., N. G. Naumov, N. Audebrand and S. Cordier, *Current Inorg. Chem.*, 2017, **7**, 111-121.
57.   K. A. Brylev, G. Pilet, N. G. Naumov, A. Perrin and V. E. Fedorov, *Eur.J. Inorg. Chem.*, 2005, 461-466.
58.   G. Daigre, K. Costuas, M. S. Tarasenko, A. Y. Ledneva, N. G. Naumov, P. Lemoine, T. Guizouarn, Y. Molard, M. Amela-Cortes, N. Audebrand and S. Cordier, *Dalton Trans.*, 2018, **47**, 1122-1130.
59.   *APEX3 program suite V2016.1-0, Bruker AXS Inc., Wisconsin, USA.*
60.   *APEX2 program suite V2014.11-0, Bruker AXS Inc., Wisconsin, USA.*
61.   *G. M. Sheldrick, SAINT Version 8.37A, 2013, Bruker AXS Inc., Wisconsin, USA.*
62.   *G. M. Sheldrick, SADABS version 2014/5, SADABS Bruker AXS Inc., Madison, Wisconsin, USA.*
63.   G. Sheldrick, *Acta Crystallogr. A*, 2015, **71**, 3-8.
64.   G. Sheldrick, *Acta Crystallogr. C*, 2015, **71**, 3-8.
65.   L. Farrugia, *J. Appl. Cryst.*, 2012, **45**, 849-854.
66.   S. J. Clark, M. D. Segall, C. J. Pickard, P. J. Hasnip, M. J. Probert, K. Refson and M. C. Payne, *Z. Kristallogr.*, 2005, **220**, 567-570.
67.   J. P. Perdew, K. Burke and M. Ernzerhof, *Phys. Rev. Lett.*, 1996, **77**, 3865-3868.
68.   A. Tkatchenko and M. Scheffler, *Phys. Rev. Lett.*, 2009, **102**, 073005.

69.   D. D. Koelling and B. N. Harmon, *J. Phys. C*, 1977, **10**, 3107-3114.

70.   S. G. Louie, S. Froyen and M. L. Cohen, *Phys. Rev. B*, 1982, **26**, 1738-1742.

71.   N. G. Naumov, A. V. Virovets, Y. I. Mironov, S. B. Artemkina and V. E. Fedorov, *Ukr. Khim. Zhurn.*, 1999, **65**, 21-27.

72.   K. A. Hofmann and F. Küspert, *Z. anorg.Chem.*, 1897, **15**, 204-207.

73.   T. Iwamoto, *J. Inclusion Phenom.*, 1996, **24**, 61-132.

74.   K. Kirakci, S. Cordier, A. Shames, B. Fontaine, O. Hernandez, E. Furet, J. F. Halet, R. Gautier and C. Perrin, *Chem. Eur. J.*, 2007, **13**, 9608-9616.

75.   S. Cordier, N. G. Naumov, D. Salloum, F. Paul and C. Perrin, *Inorg. Chem.*, 2004, **43**, 219-226.

76.   A. V. Virovets and N. V. Podberezskaya, *J. Struct. Chem. (Engl. Trans.)*, 1993, **34**, 306-322.

77.   B. Fontaine, *Structure électronique de clusters de métaux de transition de composés de l'état solide, Thesis 2006REN1S135 - Rennes 1*, 2006.

78.   Y. Molard, A. Ledneva, M. Amela-Cortes, V. Cîrcu, N. G. Naumov, C. Mériadec, F. Artzner and S. Cordier, *Chem. Mater.*, 2011, **23**, 5122-5130.

79.   L. Laffont and P. Gibot, *Mater. Charact*, 2010, **61**, 1268-1273.

80.   J. H. Rask, B. A. Miner and P. R. Buseck, *Ultramicroscopy*, 1987, **21**, 321-326.

81.   J. H. Paterson and O. L. Krivanek, *Ultramicroscopy*, 1990, **32**, 319-325.

82.   B. B. Yan, H. J. Zhou and A. Lachgar, *Inorg. Chem.*, 2003, **42**, 8818-8822.

83.   A. V. Virovets, Y. M. Gayfulin, E. V. Peresypkina, Y. V. Mironov and N. G. Naumov, *Crystengcomm*, 2015, **17**, 1477-1482.

84.   K. A. Brylev, N. G. Naumov, A. V. Virovets, S. J. Kim and V. E. Fedorov, *J. Clust. Sci.*, 2009, **20**, 165-176.